

## THE CONSEQUENCES OF HELIUM PRODUCTION ON MICROSTRUCTURAL DEVELOPMENT IN ISOTOPICALLY TAILORED FERRITIC ALLOYS - D. S. Gelles (Pacific Northwest Laboratory)<sup>a</sup>

### OBJECTIVE

The objective of this research is to assess the effect of fusion relevant He/dpa levels on microstructural development in martensitic steels for first wall applications in a fusion energy system.

### SUMMARY

A series of alloys have been made adding various isotopes of nickel in order to vary the production of helium during irradiation by a two step nuclear reaction in a mixed spectrum reactor. The alloys use a base composition of Fe-12Cr with an addition of 1.5% nickel, either in the form of <sup>60</sup>Ni which produces no helium, <sup>59</sup>Ni which produces helium at a rate of about 10 appm He/dpa, or natural nickel (<sup>Nat</sup>Ni) which provides an intermediate level of helium due to delayed development of <sup>59</sup>Ni. Specimens were irradiated in the HFIR at Oak Ridge, TN to ≈7 dpa at 300 and 400°C. Microstructural examinations indicated that nickel additions promote precipitation in all alloys, but the effect appears to be much stronger at 400°C than at 300°C. There is sufficient dose by 7 dpa (and with 2 appm He) to initiate void swelling in ferritic/martensitic alloys. Little difference was found between response from <sup>59</sup>Ni and <sup>Nat</sup>Ni. Also, helium bubble development for high helium generation conditions appeared to be very different at 300 and 400°C. At 300°C, it appeared that high densities of bubbles formed whereas at 400°C, bubbles could not be identified, possibly because of the complexity of the microstructure, but more likely because helium accumulated at precipitate interfaces.

### PROGRESS AND STATUS

#### Introduction

In order to better understand the effects of helium on embrittlement in ferritic/martensitic steels, an isotopic tailoring<sup>(1,2)</sup> approach has been taken, similar to that used to study this behavior in austenitic steels<sup>(3-5)</sup> but requiring irradiation in the HFIR. A series of alloys has been made adding various isotopes of nickel in order to vary the production of helium during irradiation by the two step nuclear reaction. The alloys use a base composition of Fe-12Cr with an addition of 1.5% nickel, either in the form of <sup>60</sup>Ni which produces no helium, <sup>59</sup>Ni which produces helium at a rate of about 10 appm He/dpa, or natural nickel which provides an intermediate level of helium due to delayed development of <sup>59</sup>Ni. Although the experiment was first envisioned over ten years ago, specimens have only now been successfully irradiated in the HFIR at Oak Ridge, TN to 10 dpa at 300 and 400°C for examination. This paper reports on microstructural differences found between these specimens irradiated under identical conditions but with the different nickel isotopes.

#### Experimental Procedure

Experimental details will be published elsewhere.<sup>(6)</sup> Specimens were irradiated in HFIR-MFE-JP23<sup>(7)</sup> The resulting fluences, taking into account specimen positions in reactor are  $3.93 \times 10^{22}$  and  $3.14 \times 10^{22}$  n/cm<sup>2</sup> for the 400 and 300°C conditions, respectively.<sup>(8)</sup> Table 1 includes estimates of dose and helium

---

<sup>a</sup>Operated for the U.S. Department of Energy by Battelle Memorial Institute under Contract DE-AC06-76RLO 1830.

accumulation based on reference 8. Note that significantly more helium is accumulated in specimens containing  $^{59}\text{Ni}$ , less for  $^{\text{Nat}}\text{Ni}$  and negligible amounts for  $^{60}\text{Ni}$  and no nickel, whereas only slight further increases in dose arise in  $^{59}\text{Ni}$  and  $^{\text{Nat}}\text{Ni}$  containing conditions, which is not the case in alloys with higher nickel content.

Table 1. Alloy Details with Irradiation Conditions Including Irradiation Temperature, Dose in dpa and Helium Production in appm, and Compositions in Weight Percent. All Other Impurities are  $\leq 0.01$  w/o.

Codes	Heat #	Nominal	Cr	Ni	C	Other	Irradiation conditions
6A5M 6A5N	E62	Fe-12Cr	11.6	na	.002	.026O <sub>2</sub>	300°C/6.5dpa/2He 400°C/7.3dpa/2He
715M 715N	R168	Fe-12Cr -1.5 $^{60}\text{Ni}$	11.7	1.32	.004	.02Si .02Mn	300°C/6.4dpa/2He 400°C/7.2dpa/2He
735M 735N	R169	Fe-12Cr -1.5 $^{59}\text{Ni}$	na	na	na	na	300°C/6.6dpa/71He 400°C/7.5dpa/77He
745M 745N	R170	Fe-12Cr 1.5 $^{\text{Nat}}\text{Ni}$	11.5	1.54	.004	.02Si .02Mn	300°C/6.5dpa/41He 400°C/7.4dpa/46He

na: not available

## Results

Microstructural damage resulting from irradiation in HFIR was only on a fine scale. Figure 1 shows low magnification examples of damage at 300 and 400°C respectively for each of the four alloys. The scale of the damage is seen as a fine background mottle. However, the mottling in specimens irradiated at 400°C is coarser than that from 300°C, and the alloy without nickel at 400°C contains mottling that is equiaxed whereas the mottling in the alloys containing nickel is non-equiaxed. Larger particles, for example those in specimen 6A5N are probably carbides, believed to have been present prior to irradiation.

As the damage is more easily understood following irradiation at the higher temperature, the microstructures formed at 400°C will first be described in greater detail. The microstructure of specimen 6A5N, Fe-12Cr, following irradiation to 7.3 dpa at 400°C and 2 appm He was found to be typical of irradiated Fe-12Cr, and contained dislocation loops, voids and precipitation typical of  $\alpha'$ , a chromium rich body centered cubic phase often formed by phase separation. An example is provided in Figure 2, comparing the same area of a specimen in  $\vec{g}=[110]$  contrast (a),  $\vec{g}=[002]$  contrast (b) and void contrast (c) for a foil near a (110) orientation. In dislocation contrast (Figures 2a and b), straight dislocations can be identified at the upper left and diagonally across the center from lower left to upper right. Also, many small black spot features can be identified representing small loops in the range 5 to 15 nm in diameter. Comparison of the two dislocation images indicates that more are present under [110] contrast, indicating the loops are generally of Burgers vector  $a < 200 >$ . In Figure 2c, a number of cavities can be identified, as large as 16 nm, but many as small as 3 nm. Of particular note is the row of three voids of intermediate size in the center that are connected to dislocations by comparison with the micrographs in dislocation contrast. Areas could be found without such dislocations, where only voids on the order of 3 nm were present. Also, in Figure 2c, a background mottling can be identified from  $\alpha'$  precipitation. This microstructural response to irradiation in HFIR was similar to that found following irradiation in fast reactors at a higher dose but the scale is finer.

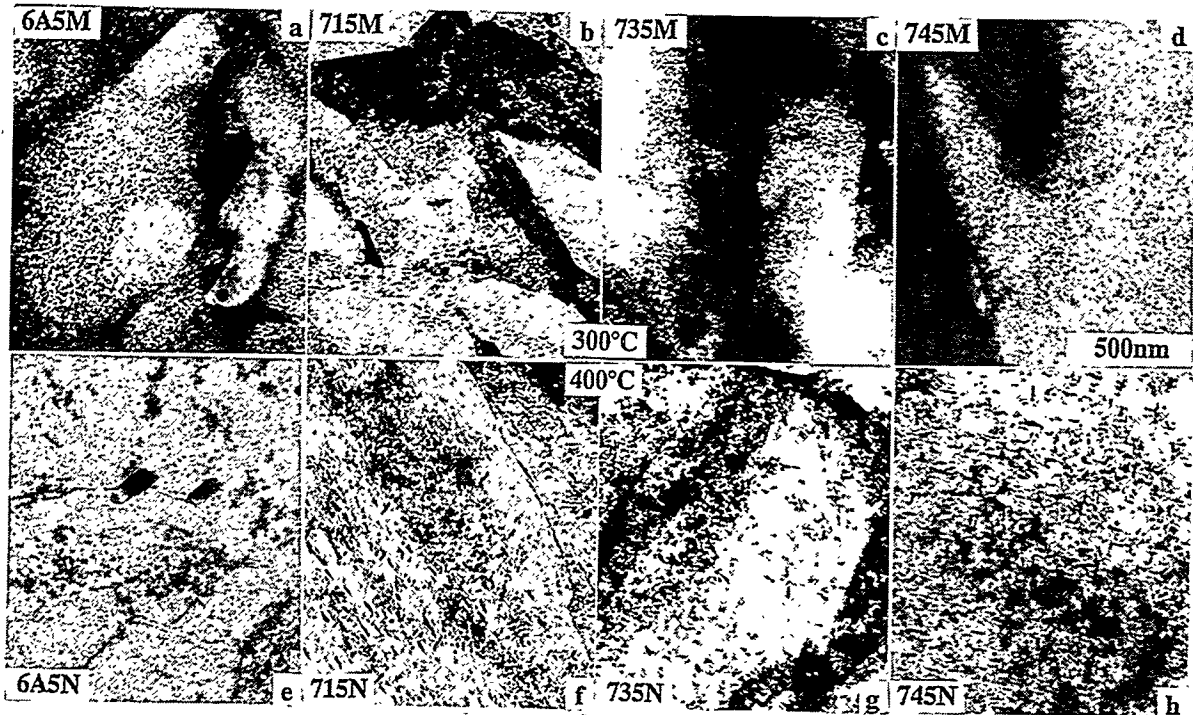


Figure 1. Microstructures in Isotopically Tailored Fe-12Cr Alloys irradiated at 300 and 400°C to 7 dpa.

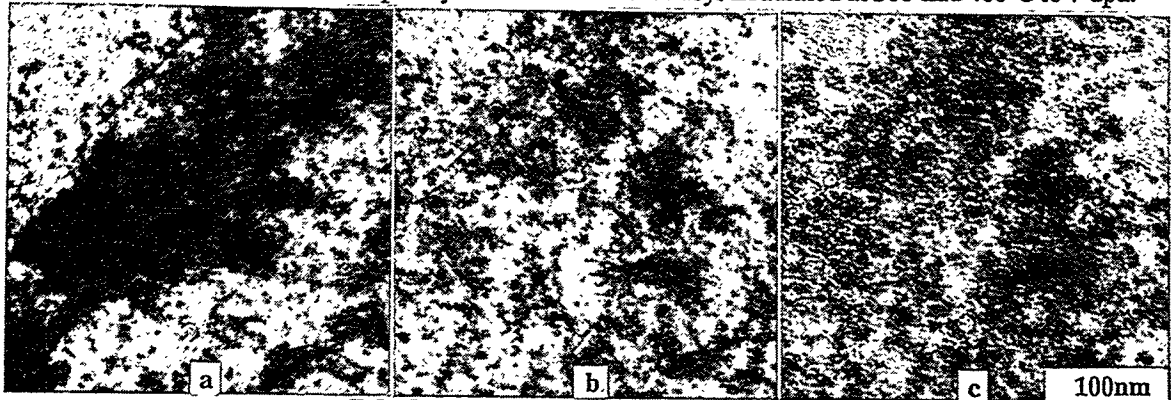


Figure 2. Fe-12Cr Specimen 6A5N Irradiated at 400°C to 7.3 dpa and 2 appm He Imaged using  $\vec{g} = [110] \uparrow$  in a),  $\vec{g} = [002] \rightarrow$  in b) and Void Contrast in c) for a Foil near  $(110)$  Orientation.

The microstructure of specimen 715N, Fe-12Cr-1.5<sup>60</sup>Ni, following irradiation to 7.2 dpa at 400°C and 2 appm He was found to be similar in some ways to irradiated Fe-12Cr, and contained dislocation loops, voids and precipitation typical of  $\alpha'$ , but loop development was significantly further advanced, examples of larger voids were not found, and a rod-shaped precipitate had developed. Examples are found in Figure 3. Again, the same area of a specimen can be compared in  $\vec{g} = [110]$  contrast (a),  $\vec{g} = [002]$  contrast (b) and void contrast (c) for a foil near a  $(110)$  orientation. Many examples of loops as large as 300 nm are seen in dislocation contrast. More loops are found under  $[002]$  contrast, but several examples can be found only under  $[110]$  contrast, indicating that both a  $\langle 100 \rangle$  and  $\frac{a}{2} \langle 111 \rangle$  Burgers vectors are present. Again straight dislocation line segments are easily identified, believed to have been present prior to irradiation. Voids can be identified in Figure 3c, ranging in size from 3 to 7 nm, but none were found as large as those in specimen 6A5N. Precipitation, similar to the equiaxed phase found in 6A5N can be found but several examples of a rod shaped phase 7 nm wide and 24 nm long can be identified. Therefore major differences arising from the addition of <sup>60</sup>Ni are larger loops, smaller maximum void diameters and the presence of a rod shaped precipitate phase.

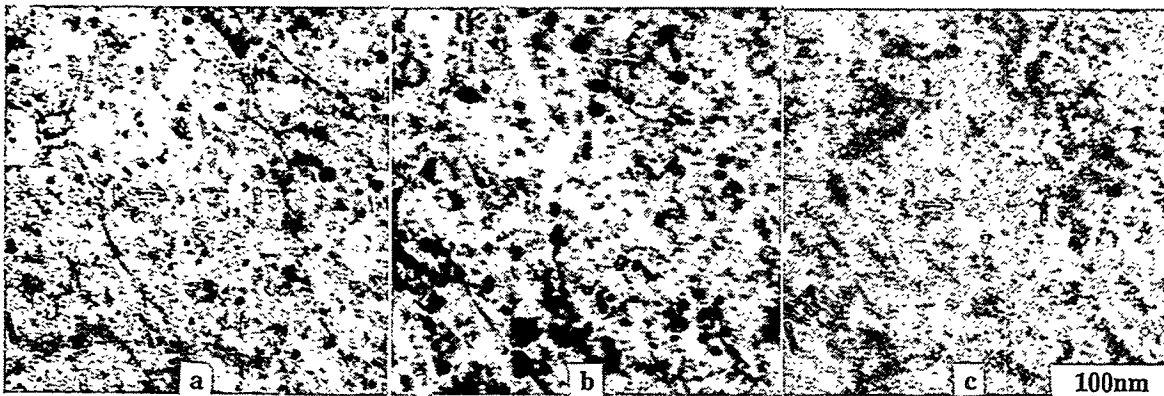


Figure 3. Fe-12Cr-1.5<sup>60</sup>Ni Specimen 715N Irradiated at 400°C to 7.2 dpa and 2 appm He Imaged using  $\vec{g} = [110] \uparrow$  in a),  $\vec{g} = [002] \rightarrow$  in b) and Void Contrast in c) for a Foil near  $(\bar{1}10)$  Orientation.

The microstructure of specimen 735N, Fe-12Cr-1.5<sup>59</sup>Ni, following irradiation to 7.5 dpa at 400°C and 77 appm He was again found to contain differences in comparison with specimens described above. The dislocation structure was similar but precipitation appeared to be more advanced and cavitation could not be identified, suggesting that it was on a much finer scale but could not be resolved. Examples are provided in Figure 4. An area is shown in  $\vec{g} = [110]$  contrast (a),  $\vec{g} = [002]$  contrast (b) and void contrast (c) for a foil near a  $(\bar{1}10)$  orientation. Loops 130 nm in diameter can be identified, and several short line segments are found which may be remnants of even larger loops. However, the dominant microstructural features are precipitates, in the form of rod shaped features as large as 20 nm wide and 60 nm long. The microstructure is so complex that it is difficult to see cavities, but if cavities are present, Figure 4c indicates that they must be less than 2 nm in diameter. Therefore, it appears that additions of helium to levels on the order of 80 appm result in enhanced accumulation of interstitials to dislocation loops, enhanced precipitation kinetics, and most probably a much finer distribution of helium bubbles.



Figure 4. Fe-12Cr-1.5<sup>59</sup>Ni Specimen 735N Irradiated at 400°C to 7.5 dpa and 77 appm He Imaged using  $\vec{g} = [110] \uparrow$  in a),  $\vec{g} = [002] \rightarrow$  in b) and Void Contrast in c) for a Foil near  $(\bar{1}10)$  Orientation.

The microstructure of specimen 745N, Fe-12Cr-1.5<sup>Nat</sup>Ni, following irradiation to 7.4 dpa at 400°C and 46 appm He was found to be similar, confirming conclusions obtained based on specimen 735N. Examples of the irradiated microstructure are in Figure 5. Again, an area is shown in  $\vec{g} = [110]$  contrast (a),  $\vec{g} = [002]$  contrast (b) and void contrast (c) for a foil near a  $(\bar{1}10)$  orientation. Loops 200 nm in diameter can be identified, and several short line segments are found which may be remnants of larger loops. The dominant microstructural features are again precipitates, in the form of rod

shaped features as large as 15 nm wide and 50 nm long. This microstructure is also so complex that it is difficult to see cavities, but if cavities are present, they are <3 nm in diameter.

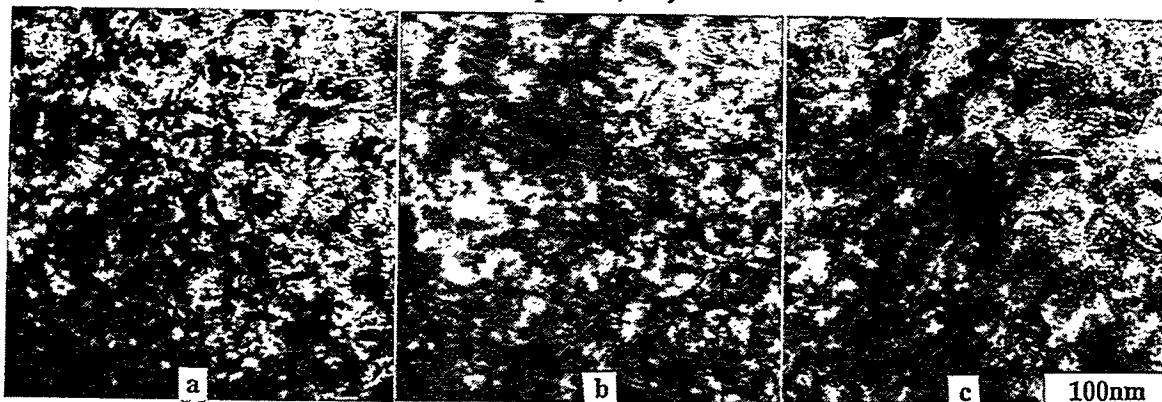


Figure 5. Fe-12Cr-1.5<sup>Nat</sup>Ni Specimen 745N Irradiated at 400°C to 7.4 dpa and 46 appm He Imaged using  $\vec{g} = [110] \uparrow$  in a),  $\vec{g} = [002] \rightarrow$  in b) and Void Contrast in c) for a Foil near  $(\bar{1}10)$  Orientation.

In order to further emphasize that nickel additions lead to precipitation Figure 6 has been prepared showing precipitate dark field images in specimens 715N and 735N. In both cases, the precipitate dark field image was taken for an orientation near (210) for  $\vec{g} \approx \frac{2}{3}(420)$  and the bright field image was without further tilt. The areas chosen include larger precipitate particles located on subgrain boundaries, to emphasize that particle growth was accelerated at boundaries. Although particle sizes for these two conditions are similar based on the dark field images, the bright field images emphasize the greater complexity that appears to arise from the added helium. Certainly, it must be concluded that nickel additions to Fe-12Cr develop complex microstructures due to precipitation.

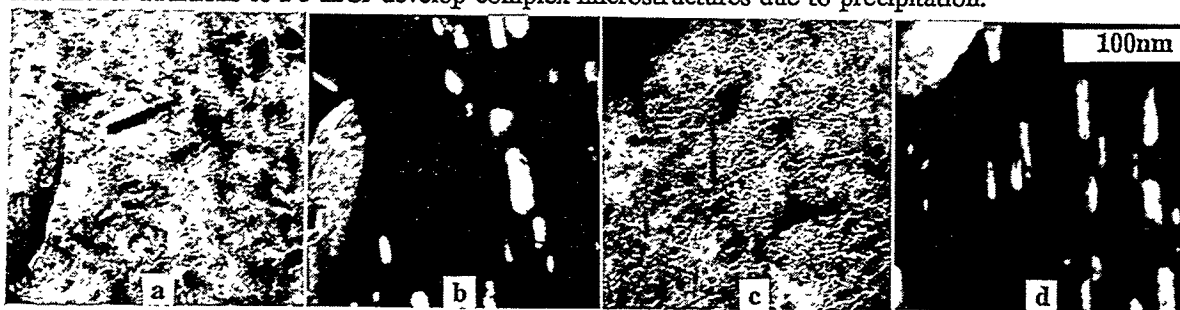


Figure 6. Bright and Dark Field Images of Precipitation in Fe-12Cr-1.5<sup>60</sup>Ni specimen 715N, a) and b), and Fe-12Cr-1.5<sup>59</sup>Ni specimen 735N, c) and d), irradiated at 400°C to  $\approx 7$  dpa.

The conclusions drawn based on specimens irradiated at 400°C are much more difficult to prove from specimens irradiated at 300°C. The scale of the irradiation induced microstructure was finer and precipitation due to the presence of nickel appeared to be significantly reduced. Of particular note was the fact that voids could be seen in specimens 735M and 745M, indicating voids as large as 3 nm, but at much higher density than at 400°C. Therefore, irradiation at 300°C appears to promote less precipitation than at 400°C, so that helium bubble formation can be observed in the high helium generating conditions.

## Discussion

These results indicate that the addition of nickel isotopes to ferritic/martensitic steels in order to provide understanding of helium effects add the complicating factor of precipitate formation, particularly for irradiation at 400°C, in interpretation of response. If precipitation is curtailed as for irradiation at 300°C, then helium bubbles develop at very high densities. But if precipitation is

extensive as for irradiation at 400°C, bubble development appears to be restricted. Therefore, effects of helium generation on ferritic/martensitic steels can better be studied with irradiation experiments at 300°C than at 400°C when helium production is from nickel transmutation.

## CONCLUSIONS

Isotopic tailoring by additions of 1.5% nickel of  $^{60}\text{Ni}$ ,  $^{59}\text{Ni}$ , and  $^{\text{Nat}}\text{Ni}$  to a base alloy Fe-12Cr have provided ferritic/martensitic alloys with very different helium levels following irradiation in the HFIR to  $\approx 7$  dpa at 300 and 400°C. Microstructural examinations revealed: 1) Nickel additions promote precipitation in all alloys, but the effect appears to be much stronger at 400°C than at 300°C. 2) There is sufficient dose by 7 dpa (and with 2 appm He) to initiate void swelling in ferritic/martensitic alloys. 3) Little difference was found between response from  $^{59}\text{Ni}$  and  $^{\text{Nat}}\text{Ni}$ . 4) Helium bubble development for high helium generation conditions appeared to be very different at 300 and 400°C. At 300°C, it appeared that high densities of bubbles formed whereas at 400°C, bubbles could not be identified, possibly because of the complexity of the microstructure, but more likely because helium accumulated at precipitate interfaces.

## Future work

The present experiment was limited by the small quantities of material available for experiments, and by the limited irradiation space available in HFIR. To provide further understanding of the effect of helium generation on deformation processes, shear punch tests will be performed on available unpolished disks. Extraction replicas are also available for each irradiated condition.

## Acknowledgements

Many have played a role allowing this experiment to reach fruition: to R. L. Simon, who first proposed the idea, with encouragement from G. R. Odette; to F. A. Garner who made the  $^{59}\text{Ni}$  available for this project and encouraged in many other ways, to P. J. Maziasz who made the  $^{60}\text{Ni}$  available and built the first HFIR irradiation experiments, to R. M. Ermi who melted the alloys, to E. M. Dieffenbacher who prepared specimens, to A. E. Ermi who organized the JP23 experiment, to J. E. Pawels, who built the JP23 experiment and distributed specimens, to A. F. Rowcliffe who fathered this experiment during its inception and to its completion, to E. M. Dieffenbacher and B. A. Walker who thinned the specimens for examinations, and finally to L. R. Greenwood who provided further understanding of the transmutation response.

## REFERENCES

- 1 R. L. Simon, in Damage Analysis and Fundamental Studies Quarterly Progress Report October-December 1982, DOE/ER-0046/12, p. 37, 1983.
- 2 G. R. Odette, J. Nucl. Matl. **141-3** (1986) 1011.
- 3 F. A. Garner, M. L. Hamilton, R. L. Simon, and M. K. Maxon, J. Nucl. Matl. **179-81** (1991) 554.
- 4 M. L. Hamilton and F. A. Garner, J. Nucl. Matl. **191-4** (1992) 1239.
- 5 M. L. Hamilton, F. A. Garner, and D. J. Edwards, J. Nucl. Matl. **212-5** (1994) 325.
- 6 D. S. Gelles, submitted for publication in 18th ASTM International Symposium on Effects of Radiation on Materials.
- 7 A. M. Ermi and D. S. Gelles, in Fusion Materials Semiannual Progress Report for the Period Ending September 30, 1994, DOE/ER-0313/17, 35.
- 8 L. R. Greenwood and R. T. Ratner, to be published in Fusion Materials Semiannual Progress Report for the Period Ending June 30, 1996, DOE/ER-0313/20.